Available online at www.sciencedirect.com
ScienceDirect
Journal of Power Sources 170 (2007) 160–172
JOURNAL OF POWER SOURCES
www.elsevier.com/locate/jpowsour

Ageing of V_2O_5 thin films induced by Li intercalation multi-cycling

Jolanta Światowska-Mrowiecka [a,*], Vincent Maurice [a], Sandrine Zanna [a], Lorena Klein [a], Emrick Briand [b], Ian Vickridge [b], Philippe Marcus [a]

[a] *Laboratoire de Physico-Chimie des Surfaces, CNRS (UMR 7045), Ecole Nationale Supérieure de Chimie de Paris, Université Pierre et Marie Curie, 11 rue Pierre et Marie Curie, 75005 Paris, France*
[b] *Institut des Nanosciences de Paris, CNRS (UMR 7588), Universités Pierre et Marie Curie et Denis Diderot, Campus Boucicaut, 140 rue de Lourmel, 75015 Paris, France*

Received 15 December 2006; received in revised form 27 March 2007; accepted 5 April 2007
Available online 12 April 2007

Abstract

Cyclic voltammetry, XPS, RBS and AFM have been combined to study the ageing mechanism of Li intercalation in V_2O_5 thin films prepared by thermal oxidation of vanadium metal. Multi-cycling tests were performed in 1 M $LiClO_4$-PC in the potential range $E \in [3.8, 2.8\,V]$ versus Li/Li^+, corresponding to the α-to-δ phase transition. XPS and AFM were performed using direct anaerobic and anhydrous transfer. Capacity fading remains inferior to 20% during ∼2500 cycles. XPS shows slight modifications of the oxide composition with a V^{4+} concentration increasing from ∼5% prior to cycling to ∼16–27% after cycling, due to Li trapped in the oxide film and to the loss of V_2O_5 active material. The presence of lithium carbonate and lithium-alkyl carbonate species evidences the formation of the so-called SEI layer. AFM evidences the loss of crystalline material by grain exfoliation from the outer V_2O_5 layer of the oxide film. By further exfoliation, the inner VO_2 layer of the oxide film is reached and pits are formed, occupying ∼9–13% of the surface. This de-cohesion at grain boundaries is attributed to the strain generated by repeated lattice distortions. After 3300 cycles, the disappearance of lithium carbonates, whereas Li-alkyl carbonates and/or Li-alkoxides remain on the surface, indicates the dissolution and/or conversion of the SEI layer. After 4500 cycles, the oxide film became very labile and could be stripped away by rinsing to reveal the vanadium metal substrate.

Keywords: Vanadium pentoxide; Lithium intercalation; Ageing; XPS; AFM; RBS

1. Introduction

Vanadium pentoxide can be used as cathode material in battery applications owing to its Li intercalation properties. The orthorhombic layered crystal structure of the α-V_2O_5 phase is characterized by weak vanadium–oxygen bonds between the layers, that allow small alkaline metal ions (M^+), like Li^+ and Na^+ [1,2] to be inserted. In the potential range between 2.5 and 3.5 V versus Li/Li^+ (the so-called "safe" potential range), the process of intercalation leads to a partial reduction of vanadium from V^{5+} to V^{4+} accompanying the insertion of 1 mol Li mol^{-1} of V_2O_5 to form the δ-LiV_2O_5 phase. At lower potentials, irreversible phase transformations occur. The structural changes of V_2O_5 were widely studied for the first time by Murphy et al. [3] and Cocciantelli et al. [4].

Cycle life is a critical parameter for the properties of Li intercalation for battery applications. Cycling the insertion and extraction of Li in the potential range indicated above induces repeated phase transitions that can cause fatigue damage to the microstructure [5,6]. However, the capacity fading observed upon ageing by multi-cycling may not originate from structural/microstructural changes only, but also from modifications of the composition of the oxide and breakdown, and/or conversion of the so-called solid electrolyte interface (SEI) layer formed at the surface [7].

The aim of the present work was to investigate the ageing of V_2O_5 thin films formed by thermal oxidation of vanadium metal. V_2O_5 thin films are interesting materials for rechargeable lithium microbatteries due to their high specific energy densities and capacities [8–13]. Many investigations concern the electrochemical properties of vanadium oxide thin films prepared by

* Corresponding author. Tel.: +33 144276736; fax: +33 146340753.
E-mail addresses: jolanta-swiatowska@enscp.fr, jeesm@agh.edu.pl (J. Światowska-Mrowiecka).

0378-7753/$ – see front matter © 2007 Elsevier B.V. All rights reserved.
doi:10.1016/j.jpowsour.2007.04.014

different method such as chemical [14–16] or physical [17–20] vapor deposition techniques and wet chemical/electrochemical [21–25] deposition methods on a variety of substrates, like glass, silicon, titanium or stainless steel. The intercalation properties of thermal oxide thin films grown on vanadium metal have recently been studied by X-ray photoelectron spectroscopy (XPS), Rutherford backscattering spectrometry (RBS), nuclear reaction analysis (NRA), atomic force microscopy (AFM), X-ray diffraction (XRD), and electrochemical methods [26–28]. Here we report on the effect of ageing by multi-cycling of these thermal oxide thin films, studied by cyclic voltammetry, XPS and AFM.

2. Experimental

The vanadium metal samples (about 11 mm in diameter and 3 mm thick) were purchased from Surface Preparation Laboratory, Zaandam, The Netherlands. They were pseudo single-crystals, oriented (1 1 1) and having a mosaic surface microstructure. The surfaces were prepared by three steps of mechanical, mechanical/chemical polishing and electropolishing, as previously described in details [26,27].

The V_2O_5 films were formed by thermal oxidation at a high O_2 pressure of 850 mbar and at $490 \pm 10\,^{\circ}C$ for 5 min in a dedicated chemical reactor (see Refs. [26,27]). For the determination of the stoichiometry of the oxide as a function of depth, Rutherford backscattering spectrometry (RBS) was used with a 2 MeV ^4He beam produced by a Van de Graaff accelerator. The detection of the backscattered ions was performed at $\theta_{lab} = 165^{\circ}$. For the latter detection angle, the depth resolution in the near surface region was better than 10 nm. The detection solid angle was around 2 msr and the beam current was set to 50 nA.

Li intercalation was performed in a glove box (Jacomex) under Ar atmosphere with H_2O and O_2 contents lower than 1ppm. The electrochemical experiments were performed using an Autolab (AUT30) and an EG&G Princeton Applied Research (Model 273) potentiostat/galvanostat. Cyclic voltammograms (CVs) were recorded in a three-electrode glass cell with V_2O_5/V(1 1 1) as working electrode and Li foil (Aldrich) as reference and counter electrodes. The electrolyte was 1 M $LiClO_4$ in propylene carbonate (1 M $LiClO_4$-PC, Aldrich). The electrodes were cycled in the safe potential range, between 2.8 and 3.8 V versus Li/Li^+, at the fast scan rate $v = 5\,mV\,s^{-1}$ and, after each set of 20 or 50 fast cycles, with a slow scan cyclic volammetry (SSCV) rate $v = 0.5\,mV\,s^{-1}$.

Two separate multi-cycling tests were performed: one up to 700 cycles and the other one up to 4500 cycles. The samples were analyzed by XPS and AFM before and after 700 cycles in the first test and before and after 1200, 2450, 3300 and 4500 cycles in the second test. All analyses were performed after Li de-intercalation at 3.8 V versus Li/Li^+. For each analysis, the sample was rinsed with acetonitrile, dried in Ar flow and directly transferred to the ultra-high vacuum XPS analysis chamber without exposure to air, using the set-up previously described [28], or analyzed by AFM under the Ar atmosphere in the glove box.

X-ray photoelectron spectroscopy (XPS) analysis was performed with a VG ESCALAB 250 spectrometer. An Al Kα monochromatized radiation ($h\nu = 1486.6$ eV) was employed as X-ray source. Binding energies were calibrated versus the carbon signal at 285.0 eV. Survey spectra were recorded with a pass energy of 100 eV and high resolution spectra of the XPS O 1s–V 2p, C 1s and valence band region were recorded with a pass energy of 20 eV.

Atomic force microscopy (AFM) imaging was performed with a Molecular Imaging instrument (PicoSPM with AFM D scanner and PicoSCAN 2100 controller) operated in contact mode, in the glove box under Ar atmosphere. The AFM images were acquired in topographic and differential modes. A silicon tip mounted on a cantilever with a force constant of 1.2–3.5 N m^{-1} was employed.

The results reported below were obtained with thermal oxide films grown on the mosaic V(1 1 1) substrate. Oxide films grown on V(1 1 1) and V(1 1 0) substrates gave quite similar XPS, AFM and RBS results and electrochemical responses allowing to exclude a significant effect of the substrate structure on the intercalation properties of the oxide film. Also, the electrochemical response of a blank sample stored for 1 month in the glove box was similar to that of a pristine sample indicating no ageing.

3. Results

3.1. Stoichiometry of the oxide film

In order to investigate the oxide composition as a function of depth, RBS analyses were performed on the sample used in the 4500 cycle test. The energy spectrum of the backscattered ions is presented in Fig. 1. The oxide compositions were extracted as a function of depth by a fitting procedure, using the SIMNRA

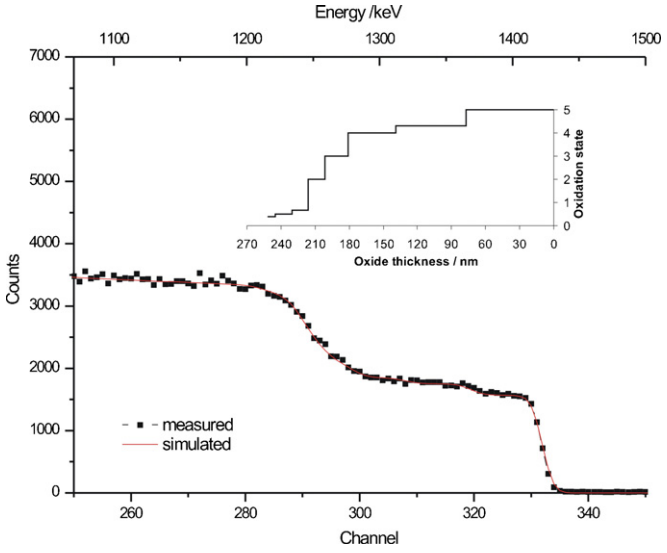

Fig. 1. RBS spectrum of the pristine film. The inset shows the oxide composition as a function of depth obtained by fitting the RBS spectrum. The fit is represented in full line, along with the data. The oxidation state is deduced from the stoichiometry used in the simulation.

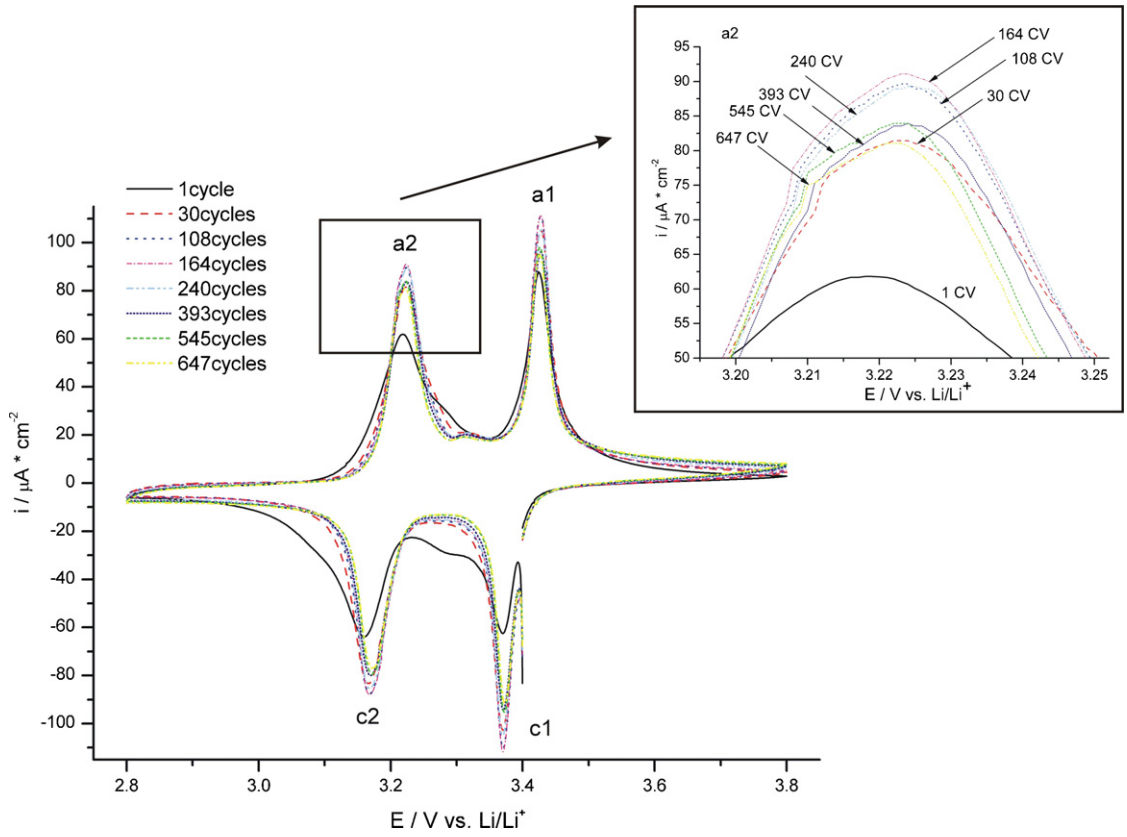

Fig. 2. Slow scan cyclic voltammograms (SSCV's) for V_2O_5/V(1 1 1) in the potential range $E \in [3.8, 2.8\ V]$ vs. Li/Li^+ in 1 M $LiClO_4$-PC, scan rate $v = 0.5\ mV\ s^{-1}$.

software. Absolute calibration of solid angle was obtained by using a reference consisting of a known amount of Bi implanted in a pre-amorphised Si target. Very good fits of the experimental spectra were obtained when assuming the depth profiles shown in the inset. In this representation, the depth, expressed in nm, was obtained from the areal densities given by the fitting procedure by using the known volumic densities of the different oxides. Note that the fitting is obtained by setting a stoichiometry at each depth that can correspond either to a certain crystalline oxide phase or to a mixture of phases. The oxide consists of V_2O_5 in the outermost layer (~77 nm thick) and a VO_2 layer below (~42 nm thick). Between these oxides, mixed oxides of type V_nO_{2n+1} can be formed. A good fit is obtained by assuming that they correspond to ~61 nm of V_6O_{13}. Underneath the VO_2 layer, the oxide composition changes gradually, passing over a wide range of oxidation states and finally including oxygen diffusion into the metal. The overall thickness of the oxide film was about 220 nm.

3.2. Electrochemical cycling tests

Fig. 2 shows a selection of SSCV's for V_2O_5/V(1 1 1) in 1 M $LiClO_4$-PC obtained during the 700 cycle test. Two sets of cathodic/anodic peaks, c1/a1 and c2/a2, are observed at $E = 3.38$ V (c1), $E = 3.42$ V (a1) and at $E = 3.18$ V (c2), at $E = 3.21$ V (a2). They evidence that Li intercalation is quasi-reversible in this range of potential ($E \in [2.8, 3.8\ V]$). The c1/a1 and c2/a2 peaks correspond to the insertion/de-insertion of Li ions into the α-V_2O_5 oxide lattice to form ε and δ phases, respectively, according to the following two reactions [3,4,29]:

$$c1/a1: \quad V_2O_5 + (1/2)Li^+ + (1/2)e^- \Leftrightarrow Li_{0.5}V_2O_5 \qquad (1)$$

$$c2/a2: \quad Li_{0.5}V_2O_5 + (1/2)Li^+ + (1/2)e^- \Leftrightarrow LiV_2O_5 \qquad (2)$$

The very well defined cathodic and anodic peaks provide an indirect evidence of the crystalline quality of the oxide film produced by thermal oxidation of vanadium metal in agreement with previous XRD and AFM data [26,27] and also with the AFM data reported below. The peaks progressively became sharper and stabilized after ~30 cycles, and remained relatively stable for the next 100–130 cycles before decreasing in intensity.

Fig. 3 shows the evolution of the charge density (normalized to the initial values of 29.6 and 29.06 mC cm^{-2} for anodic and cathodic part, respectively) with cycling. The capacity cannot be precisely deduced for this particular sample, as the thickness of the oxide layer was not measured. The evolution shows an increase of 3% during the first ~100 cycles and a continuous decrease afterwards. It is assumed that minor changes of the oxide morphology and/or structure are electrochemically activated during the first cycles, which allows a few percents increase of the capacity. The fading measured after 700 cycles corresponds to 16% of the initial value.

Fig. 4 shows the evolution of the charge density (normalized to the initial values of 17.72 and 16.82 mC cm^{-2} for anodic and cathodic part, respectively) with cycling in the 4500 cycle test. Taking into account the thickness of 77 nm of the outer V_2O_5

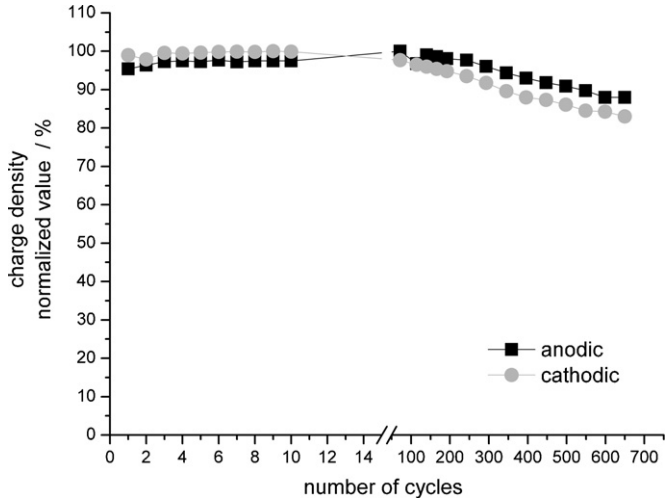

Fig. 3. Charge density evolution (normalized value) vs. number of cycles in the 700 cycle test. The values were calculated from the area of cathodic (intercalation) and anodic (de-intercalation) peaks in the SSCV's.

layer measured by RBS on this sample, the initial charge density corresponds to a capacity of 182 mAh g^{-1}. This is larger than the theoretical value of 147 mAh g^{-1} that corresponds to the formation of the δ phase (LiV_2O_5). This excess of charge indicates that Li also intercalates in the V_6O_{13} inner layer of the oxide film. The capacity loss on this sample was 9% after 700 cycles. After ∼1200 cycles, the loss was 18% of the initial value. The capacity was then nearly stable until 2450 cycles. It decreased afterwards and dropped to about 75% of the initial value after 3300 cycles at which stage it remained nearly stable until the end of the test (4500 cycles).

3.3. Chemical changes of the oxide film

Fig. 5 presents the XP V 2p and O 1s core level spectra for the V_2O_5/V(1 1 1) thin film prior and after the 700 cycle test. Binding energies (E_B) and full-widths at half-maximum

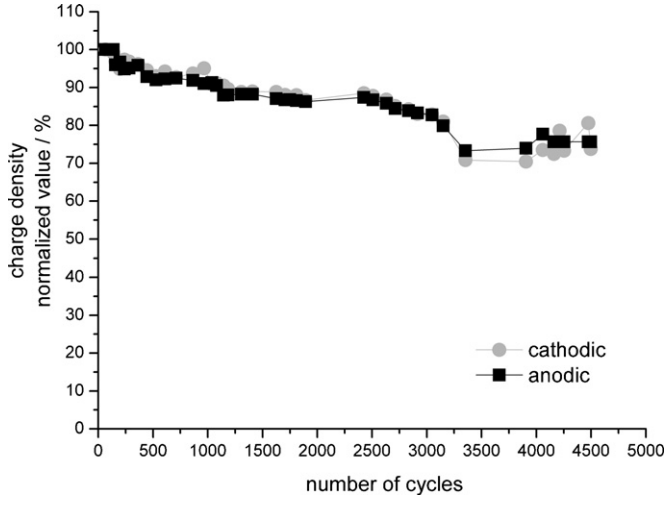

Fig. 4. Charge density evolution (normalized value) vs. number of cycles in the 4500 cycle test. The values were calculated from the area of cathodic (intercalation) and anodic (de-intercalation) peaks in the SSCV's.

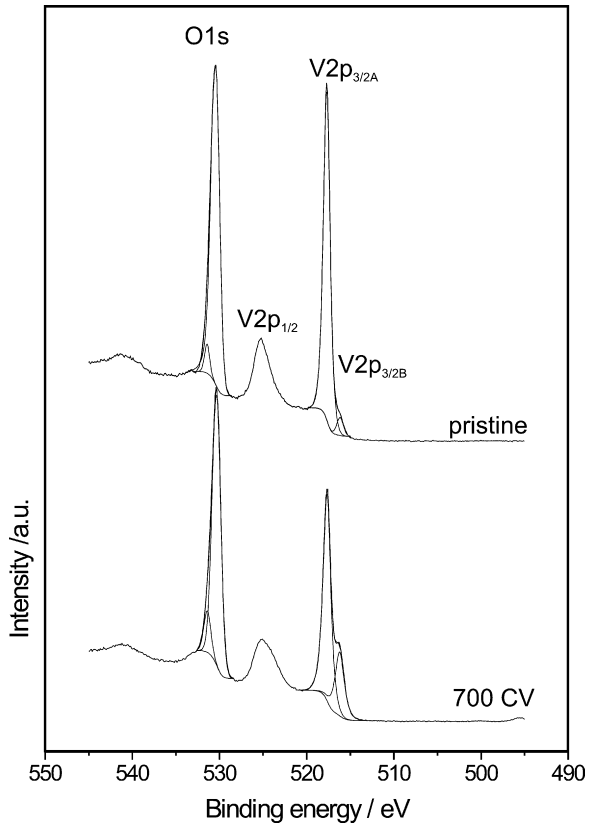

Fig. 5. XP spectra of the V 2p and O 1s core levels for a V_2O_5/V(1 1 1) thin film prior to cycling and after 700 cycles.

(FWHM) values are compiled in Table 1. For the pristine film, the V $2p_{3/2}$ and O 1s core levels are at E_B(V $2p_{3/2A}$) = 517.86 eV, E_B(V $2p_{3/2B}$) = 516.33 eV and E_B(O $1s_A$) = 530.61 eV. The two components of the V $2p_{3/2}$ peak located at 517.86 and 516.33 eV are related to two oxidation states, V^{5+} and V^{4+}, respectively, in agreement with previous data [26–28]. The proportion of V^{5+} ($V^{5+}/(V^{5+} + V^{4+})$) is 95%, indicating that the outer surface of the oxide film consists mostly of V^{5+}. The O $1s_A$ peak is assigned to the oxygen ions of the oxide layer.

The stoichiometry of the oxide film can be calculated from the peak area at E_B(V $2p_{3/2A}$) = 517.86 eV and E_B(O $1s_A$) = 530.61 eV as previously described [28]. The measured O/V atomic concentration ratio is 2.53, which confirms the formation of V_2O_5. An additional oxygen component at E_B(O $1s_B$) = 531.42 eV can be ascribed to the surface contamination

Table 1
Binding energy (E_B) and the full-width at half-maximum (FWHM) in the XPS spectra of O 1s and V 2p for a V_2O_5/V(1 1 1) thin film prior to and after 700 cycles in the potential range $E \in [3.8, 2.8\ V]$ vs. Li/Li^+ in 1 M $LiClO_4$-PC

	Pristine		700 CV	
	E_B (eV)	FWHM (eV)	E_B (eV)	FWHM (eV)
O $1s_A$	530.61	1.10	530.35	1.20
O $1s_B$	531.42	1.04	531.37	1.10
O $1s_C$	–	–	–	–
V $2p_{3/2A}$	517.86	0.93	517.67	1.15
V $2p_{3/2B}$	516.33	0.88	516.17	1.24

(C–O, O=C–O and/or O=C–N bonds [30]). The surface of these V_2O_5/V(1 1 1) thin films is quite similar to that of the V_2O_5/V(1 1 0) thin films [28].

After 700 cycles of Li intercalation/de-intercalation, the V 2p core level spectrum reveals chemical changes of the thin oxide film (Fig. 5). An increase of the intensity of the V $2p_{3/2B}$ peak (V^{4+}) and a decrease of the intensity of the V $2p_{3/2A}$ peak (V^{5+}) are observed. This change of relative intensities evidences the reduction and/or loss of V^{5+} ions with a resulting concentration of 77% V^{5+} and 23% V^{4+}. There is no signal from the vanadium metal substrate (E_B = 512.4 eV [26]), which confirms that the oxide film still forms a thick layer covering the metal surface.

The FWHM values of the V 2p peaks also vary (Table 1). The V $2p_{3/2A}$ and V $2p_{3/2B}$ FWHM values increase from 0.93 to 1.15 eV and from 0.88 to 1.24 eV, respectively, after 700 cycles. The low values for the pristine surface are consistent with the formation of well-crystallized films [20,31,32]. Their increase after cycling is an indication of structural changes, due to distortion of the oxide lattice.

The O 1s core level spectrum does not show major changes after 700 cycles. A slight increase of O $1s_A$ and O $1s_B$ FWHM values is observed (Table 1). The presence of contaminants like carbonates (expected component at E_B(O 1s) ≅ 533 eV), usually observed on the surface as a result of the electrolyte decomposition [7,20,28], is not clearly evidenced in this case.

Fig. 6 presents the XP V 2p and O 1s core level spectra obtained prior to and after 1200, 2450 and 3300 cycles during the 4500 cycle test. Binding energies and FWHM values are compiled in Table 2. On this sample, the pristine oxide film is 96% V^{5+} and 4% V^{4+}. After cycling, the spectra confirm a modified surface composition of the oxide film. The V^{4+} content is 27, 16 and 18% after 1200, 2450 and 3300 cycles, respectively. The lower values obtained after 2450 and 3300 cycles suggest that after 1200 cycles an excess of Li ions remained intercalated in the oxide but was not irreversibly trapped. After 1200 cycles, the increase of the V 2p FWHM from 0.93 to 1.26 eV for V $2p_{3/2A}$ and from 0.90 to 1.25 eV for V $2p_{3/2B}$ confirms the alteration of the structure. The lower values obtained after 2450 and 3300 cycles (1.13 and 1.10 eV, respectively for the V $2p_{3/2A}$ peak) support the interpretation that the high amount of V^{4+} obtained after 1200 cycles was related to an excess of intercalated Li ions distorting the oxide lattice.

The valence band (VB) region prior to and after 1200, 2450 and 3300 cycles is presented in Fig. 7. The spectra show a Li 1s peak at E_B(Li 1s) = 56.06 eV that reveals the presence of intercalated Li ions, in agreement with the reduction of V^{5+} to V^{4+}. The higher intensity of the Li 1s peak is consistent with the higher proportion of V^{4+} ions remaining intercalated after 1200 cycles. The VB region also shows that the V 3p core level peaks are broader due to the presence of two components at E_B(V $3p_A$) = 42.62 eV and at E_B(V $3p_B$) = 40.24 eV corresponding to V^{5+} and V^{4+}, respectively. Fig. 7 also shows that Li, intercalated in the oxide after cycling, induces an additional photoemission located at E_B(V 3d) = 1.3 eV. This observation evidences a modified electronic structure caused by Li intercalation. The empty V 3d states of the V^{5+} ions are filled by the electrons transferred from 2s levels of intercalated Li to form V^{4+} ions. The presence

Table 2
Binding energy (E_B) and full-width at half-maximum (FWHM) for the XP O 1s, C 1s and V 2p peaks for a V_2O_5/V(1 1 1) thin film prior to and after 1200, 2450, 3300 and 4500 (Points 1–3) cycles in the potential range $E \in$ [3.8, 2.8 V] vs. Li/Li^+ in 1 M $LiClO_4$-PC

	Pristine		1200 CV		2450 CV		3300 CV		4500 CV Point 1		4500 CV Point 2		4500 CV Point 3	
	E_B (eV)	FWHM (eV)	E_B (eV)	FWHM (eV)	E_B (eV)	FWHM (eV)	E_B (eV)	FWHM (eV)	E_B (eV)	FWHM (eV)	E_B (eV)	FWHM (eV)	E_B (eV)	FWHM (eV)
O $1s_A$	530.16	1.14	530.20	1.20	530.48	1.16	530.36	1.20	530.30	1.24	530.27	1.16	530.24	1.10
O $1s_B$	530.93	1.19	531.20	1.30	531.49	1.30	531.18	1.24	531.40	1.29	531.23	1.23	531.16	1.30
O $1s_C$	–	–	532.40	1.10	532.32	1.30	532.16	1.24	532.20	1.12	532.35	1.29	532.52	1.25
O $1s_D$	–		–	–	–	–	533.58	1.29	533.01	1.23	533.56	1.29	533.63	1.15
C $1s_A$	285.00	1.19	285.00	1.55	285.00	1.57	285.00	1.58	285.00	1.60	285.00	1.59	285.00	1.42
C $1s_B$	286.34	1.32	286.32	1.55	286.43	1.60	286.53	1.60	286.51	1.63	286.52	1.49	286.51	1.60
C $1s_C$	289.04	1.20	287.99	1.50	287.93	1.58	288.30	1.56	288.57	1.60	288.02	1.51	288.71	1.60
C $1s_D$			290.16	1.49	290.1	1.55			289.97	1.47	289.72	1.54	291.66	1.59
V $2p_{3/2A}$ (V^{5+})	517.41	0.93	517.32	1.26	517.59	1.13	517.67	1.10	517.44	1.06	517.55	1.07	517.64	1.31
V $2p_{3/2B}$ (V^{4+})	515.90	0.90	515.77	1.25	516.07	1.13	516.18	1.09	516.20	1.30	516.04	1.06	516.12	1.22
V $2p_{3/2C}$ (V^{3+})	–	–	–	–	–	–	–	–	515.14	1.25	–	–	–	–
V $2p_{3/2D}$ (V^{2+})	–	–	–	–	–	–	–	–	513.77	1.20	–	–	–	–
V $2p_{3/2E}$ (V^0)	–	–	–	–	–	–	–	–	512.55	0.90	–	–	–	–

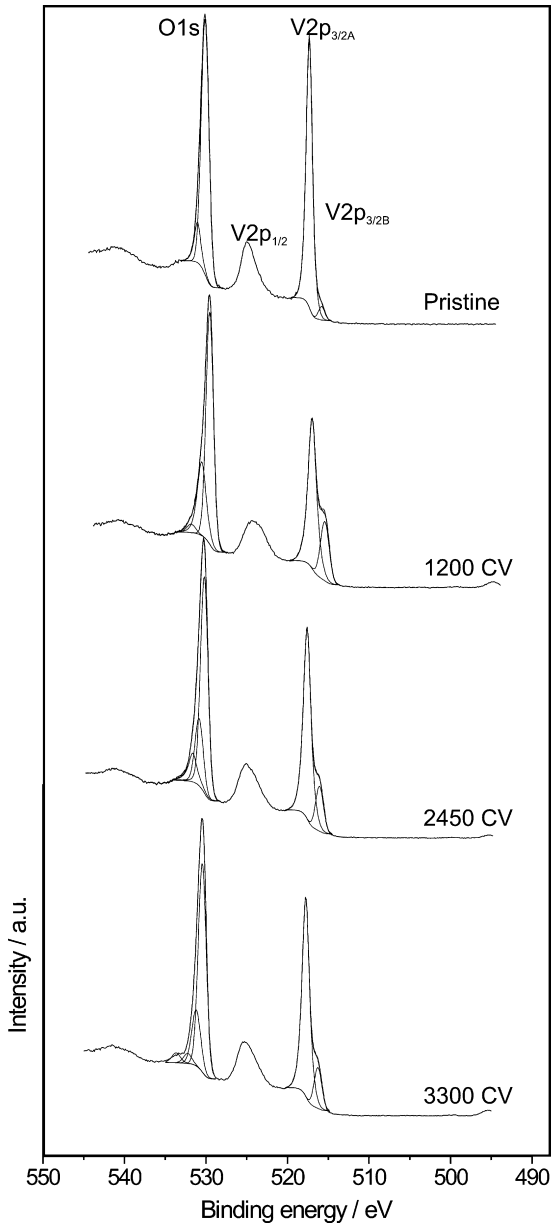

Fig. 6. XP spectra of the V 2p and O 1s core levels for a V_2O_5/V(1 1 1) thin film prior to cycling and after 1200, 2450, and 3300 cycles.

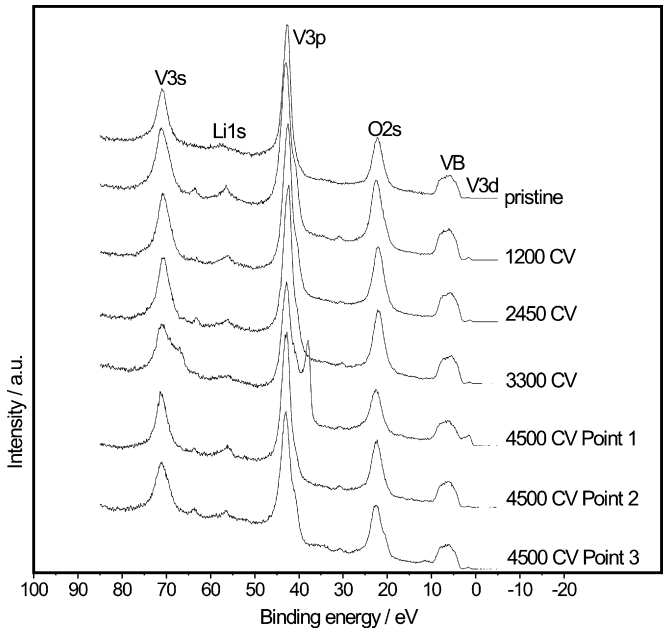

Fig. 7. XP spectra of the VB region for V_2O_5/V(1 1 1) prior to cycling and after 1200, 2450, 3300 and 4500 cycles.

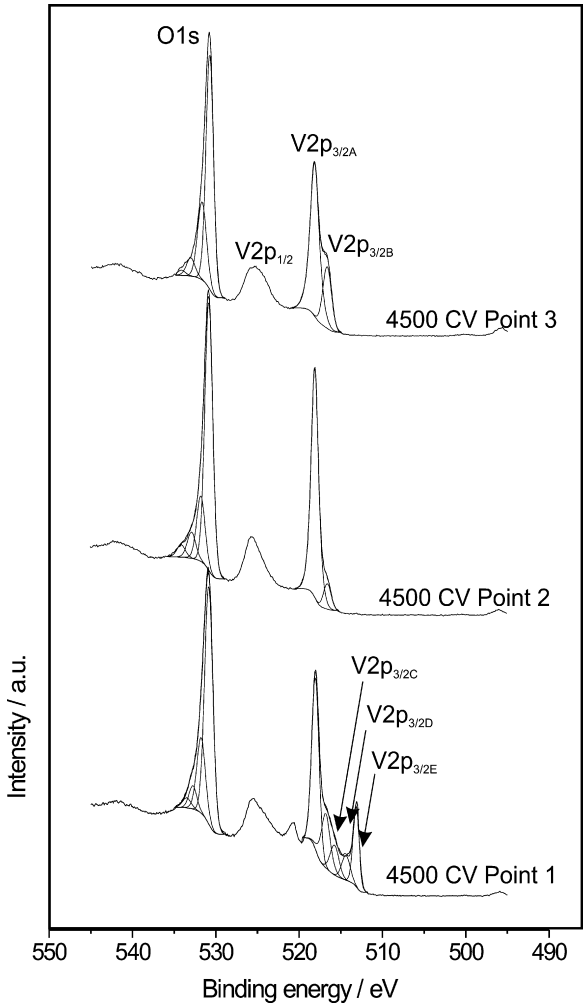

Fig. 8. XP V 2p and O 1s core level spectra for the V_2O_5/V(1 1 1) after 4500 cycles.

of the Li 1s peak, the broadening of the V 3p peak and the appearance of the V 3d peak confirm the irreversible modification of the thin oxide film, also evidenced by the V 2p peaks.

Fig. 8 presents the XP V 2p core level spectra obtained after 4500 cycles. At this stage of multi-cycling, visual inspection showed an heterogeneous surface after emerging the sample from the solution. Metallic parts of the sample were revealed by stripping of the oxide film after rinsing the surface with acetonitrile. It cannot be excluded that the repeated stages of *ex situ* transfer and rinsing of the electrode amplified the degradation of the oxide film. The surface was analyzed in three different points selected with the optical camera in the XPS analysis chamber. Point 1 (Fig. 8; Table 2) corresponds to a site where the thin oxide film was the most deteriorated. The V $2p_{3/2}$ core level spectrum consist of five peaks: V $2p_{3/2A}$, V $2p_{3/2B}$, V $2p_{3/2C}$, V

$2p_{3/2D}$, V $2p_{3/2E}$, corresponding to V^{5+}, V^{4+}, V^{3+}, V^{2+} and V^0, respectively. The surface content, in this location, is 56% V^{5+}, 23% V^{4+}, 12% V^{3+}, 1% V^{2+} and 8% V^0. Point 2 corresponds to a well-preserved V_2O_5 film according to XPS (Fig. 8; Table 2) with 91% V^{5+} and 9% V^{4+}. Point 3 shows a modified oxide film consisting of 74% V^{5+} and 26% of V^{4+} (Fig. 8; Table 2).

It can be seen in Fig. 7 that the spectra of the VB region for Points 2 and 3 are quite similar to the spectra obtained after 2450 and 3300 cycles. The spectra obtained in Point 1 is significantly different due to presence of vanadium metal on the surface. Additional peaks are observed at E_B(V 3s) = 66.19 eV and E_B(V 3p) = 37.19 eV corresponding to metallic V^0, in agreement with the V 2p spectrum. The intense peak observed at E_B(V 3d) = 1.3 eV is also consistent with the presence of metallic vanadium on the surface suggesting a complete exfoliation of the film in these sites. The loss of vanadium oxide is confirmed by the lower intensity of the Li 1s peak.

3.4. Formation of the SEI layer

Fig. 9 presents the XP C 1s core level spectra prior to and after 1200, 2450 and 3300 cycles. Binding energies and FWHM values are compiled in Table 2. Three components are observed on the pristine film. The main one, set at E_B(C $1s_A$) = 285 eV, is assigned to hydrocarbons, $–CH_2CH_2–$, always detected at the extreme surface. The second one at E_B(C $1s_B$) = 286.34 eV can be assigned to C–O bonds. The third one at E_B(C $1s_C$) = 289.04 eV corresponds to O=C–O or O=C–N species. The nitrogen peak observed at E_B(N 1s) = 402.01 eV is consistent with the presence of O=C–N species but O=C–O species cannot be excluded. Consistently, the O 1s peak observed at E_B(O $1s_B$) = 530.93 eV can originate from C–O bonds and/or O=C–N/O=C–O species [30].

After 1200 and 2450 cycles, a different component at E_B(C $1s_C$) ≅ 288 eV and a new component at E_B(C $1s_D$) ≅ 290 eV are observed. They are assigned Li-alkyl carbonates ($ROCO_2Li$) [33,34] and/or Li-alkoxides (R-CH_2OLi) [35] and lithium carbonates (Li_2CO_3), respectively [20,33,34]. These components were already observed during the first intercalation cycle in this safe potential range, as shown in our previous study [28]. The oxygen peak, corresponding to lithium carbonates, is observed at E_B(O $1s_B$) = 531.20 and 531.49 eV after 1200 and 2450 cycles, respectively. The oxygen peak, corresponding to ($ROCO_2Li$) and/or Li-alkoxides (R-CH_2OLi), is observed at E_B(O $1s_C$) = 532.40 and 532.32 eV after 1200 and 2450 cycles, respectively.

The two other C 1s components, detected on the pristine film at E_B(C $1s_A$) = 285 eV ($–CH_2CH_2–$) and E_B(C $1s_B$) = 286.32/286.43 eV (C–O), are still observed after 1200 and 2450 cycles. However, the increased intensity of the C $1s_B$ component after electrochemical treatment indicates the uptake of contamination (C–O bonds) at the surface. We can also note a significant increase of the FWHM values for all the C 1s components after the electrochemical treatment. All these changes are characteristic of the formation of the SEI layer [20,28,36,37].

After 3300 cycles, only three peaks are observed in the C 1s core level spectrum at E_B(C $1s_A$) = 285 eV ($–CH_2CH_2–$), E_B(C $1s_B$) = 286.53 eV (C–O) and E_B(C $1s_C$) = 288.30 eV ($ROCO_2Li$ and/or R-CH_2OLi). The C $1s_B$ and C $1s_C$ peaks have lower intensities than before. The C $1s_D$ peak (Li_2CO_3) is absent. The oxygen peak at E_B(O $1s_B$) = 531.18 eV can be assigned to contamination (C–O, O=C–O bonds) in the absence of the C 1s signal corresponding to Li_2CO_3. The oxygen peak at E_B(O $1s_C$) = 532.16 eV ($ROCO_2Li$ and/or R-CH_2OLi) is observed with a lower intensity in agreement with variation of the C

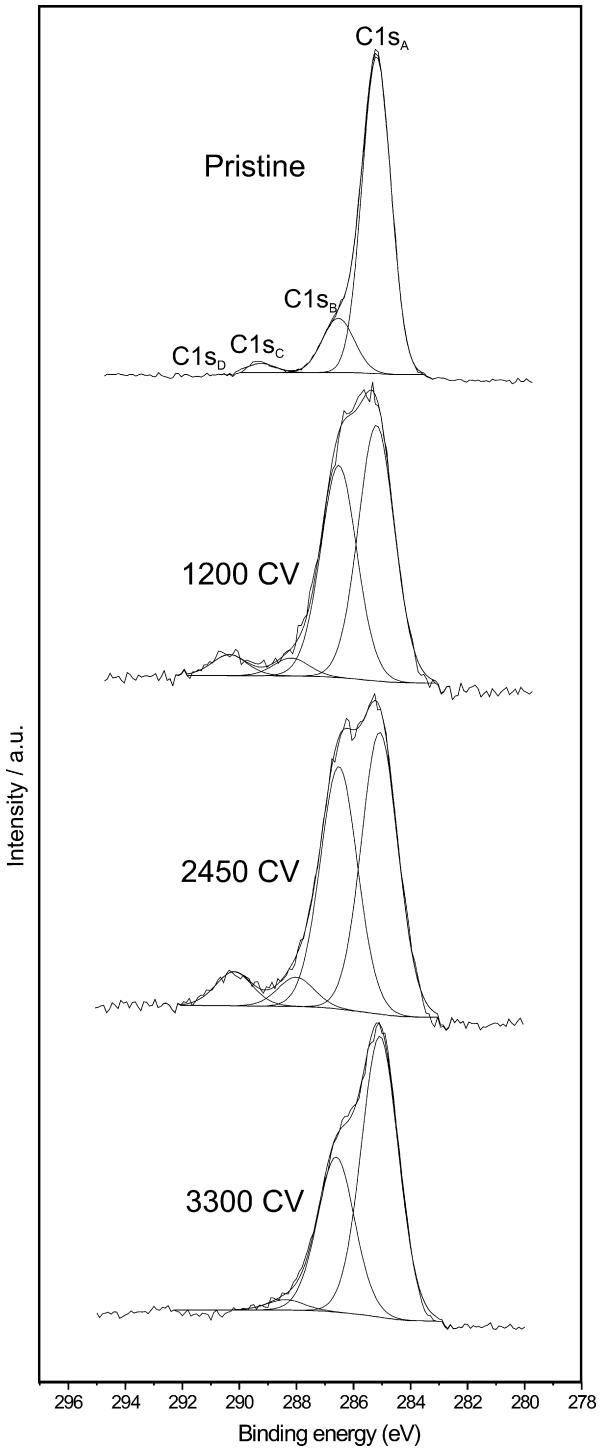

Fig. 9. XP C 1s core level spectra for V_2O_5/V(1 1 1) prior to cycling and after 1200, 2450 and 3300 cycles.

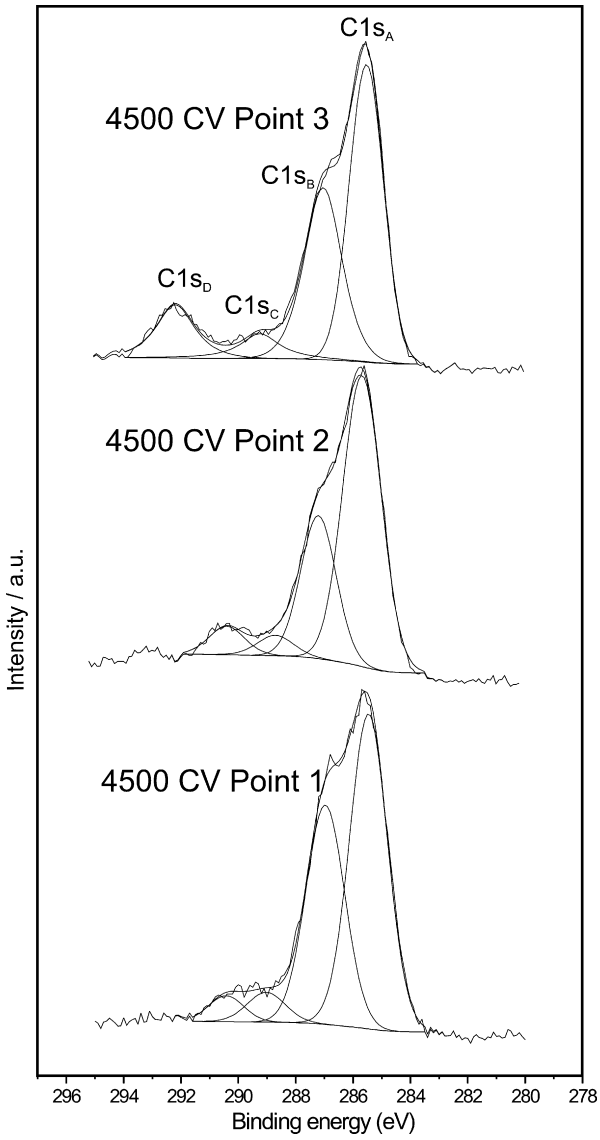

Fig. 10. XP C 1s core level spectra for V_2O_5/V(1 1 1) after 4500 cycles.

1s$_C$ peak. A low intensity peak at E_B(O 1s$_D$) = 533.56 eV is also observed. These variations suggest the dissolution and/or conversion of the SEI layer after 3300 cycles.

After 4500 cycles, the C 1s spectrum measured on Point 2 (Fig. 10), which corresponds to the area where the V_2O_5 is well preserved (91% V^{5+}), shows four carbon peaks similar to those observed after 1120 and 2450 cycles. The same characteristics are also observed in the O 1s core level region. Like after 3300 cycles, the small intensity oxygen peak at E_B(O 1s$_D$) = 533.56 eV is assigned to contaminations derived from the cell set-up.

In Point 1, where the vanadium metal substrate was revealed due to the deterioration of the oxide film, four carbon peaks are observed. The peak at E_B(C 1s$_C$) = 288.57 eV ($ROCO_2Li$ and/or R-CH_2OLi) is shifted by about 0.5 eV to higher binding energies, compared to the previous analyses. It could result from the contribution of C=O adsorbed on the metal surface. The oxygen peak corresponding to C=O species would overlap the oxygen peak corresponding to Li-alkyl carbonates and/or Li-alkoxides in the component at E_B(O 1s$_C$) = 532.20 eV. The oxygen peak at E_B(C 1s$_D$) = 533.01 eV is also observed.

On Point 3, corresponding to 84% V^{5+} in the oxide film, a highly contaminated surface was observed. The survey spectrum revealed high intensity peaks for Na and F. In this case, it is assumed that the carbon peak now at E_B(C 1s$_D$) = 291.66 eV is related to Teflon (–CF_2CF_2–) originating from the electrochemical cell. The peak related to Li-alkyl carbonates and/or Li-alkoxides is located at E_B(C 1s$_C$) = 288.71 eV. Similarly to Points 1 and 2, the component at E_B(O 1s$_D$) = 533.63 eV corresponds to some contamination or species connected with the modification of SEI layer. These measurements confirm the inhomogeneous character of the sample surface after 4500 cycles of Li intercalation/de-intercalation.

3.5. Microstructural changes

Fig. 11 shows an AFM image of the pristine V_2O_5/V(1 1 1) sample used in the 700 cycle test. The surface is rough due to the oxidation treatment. Indeed, the z-range (max-to-min height) is 40 nm compared to 2 nm for the electropolished metal surface prior to the oxidation treatment [26]. The RMS roughness

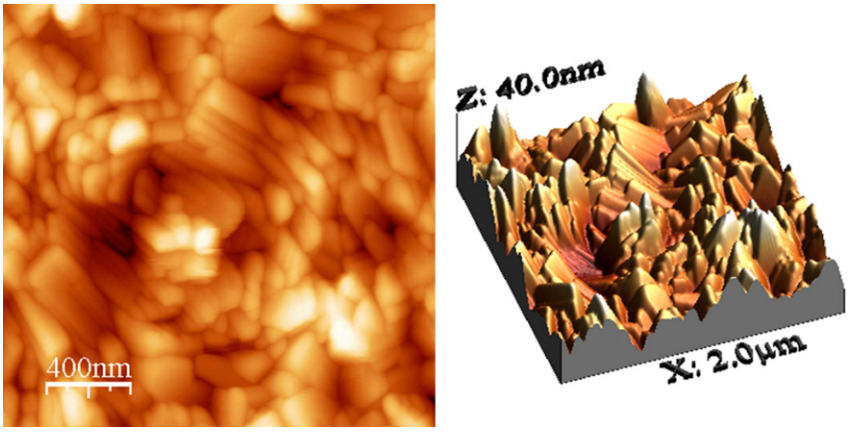

Fig. 11. Topographic AFM image for the pristine V_2O_5/V(1 1 1) film. Topview (left) and 3D view (right).

is 6 nm. The oxide film consists of grains ranging from 40 to 200 nm in lateral size. The grains have sharp edges producing well-marked grain boundaries, which confirms the crystallization of the oxide film.

Fig. 12 shows three AFM images of the oxide surface after 700 cycles of Li intercalation/de-intercalation. The larger view in Fig. 12a shows that the oxide layer is no longer uniform and presents pits. Fig. 12b shows the oxide microstructure between two pits. The RMS roughness between two pits is 10 nm, larger than that measured on the pristine oxide surface. No marked difference is observed with the granular structure observed prior to cycling. However, the grain boundaries appear less well-marked after the electrochemical treatment as revealed by the comparison of the images in Figs. 11 and 12b. Fig. 12c shows the structure observed inside and around one pit. A grain microstructure is also observed inside the pit and the pit edge is well-marked, most likely running along grain boundaries of the oxide film. This shows that the pits result from the exfoliation of the oxide grains. The depth profile of this pit indicates an average height difference of ~95 nm between the bottom of the pit and the surface of the oxide film. This is lower that the total thickness of the outer part of the oxide film containing V^{5+} and V^{4+} ions

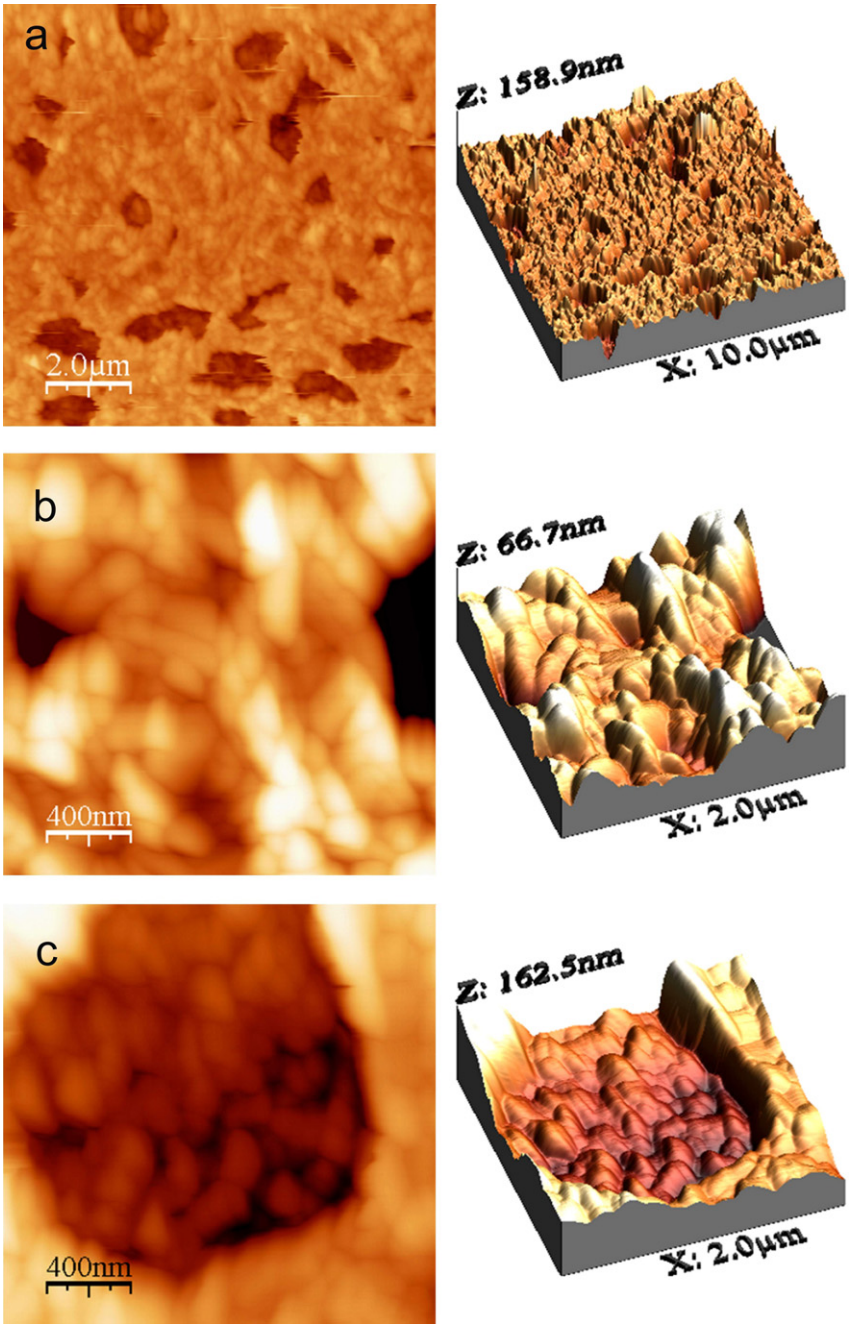

Fig. 12. Topographic AFM images of the V_2O_5/V(1 1 1) thin film after 700 CVs: (a) 10 μm × 10 μm, (b) 2 μm × 2 μm, and (c) 2 μm × 2 μm. Topview (left) and 3D view (right).

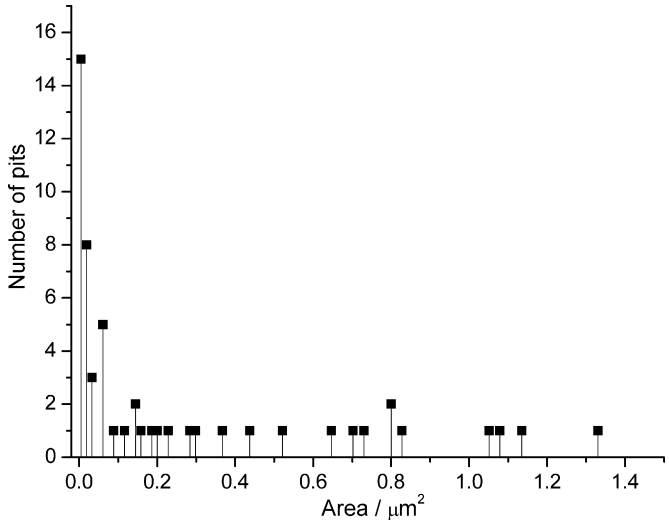

Fig. 13. Pit area histogram calculated from the AFM image in Fig. 12a by selecting a minimum depth of the pits of 50 nm and minimum area of 0.0015 μm^2.

which, according to the RBS data for the sample used for the 4500 cycle test, is ~180 nm thick. This indicates that the exfoliation of the grains forming the pits proceeds inwards through the oxide film without reaching the metal/oxide interface nor the inner part containing V^{3+} and lower ions, in agreement with the XPS data that do not indicate the presence of these vanadium oxidation states at this stage. The RMS roughness measured at the bottom of the pit is 10 nm, which is similar to the oxide surface outside the pits.

Fig. 13 shows the histogram of the pit area calculated from Fig. 12a. The pit area is relatively large and can reach more than 1 μm^2. There are 11 pits with the area larger than 0.5 μm^2, 4 pits with an area from 0.2 to 0.8 μm^2 and 38 pits with an area smaller than 0.2 μm^2. This confirms that most pits result from the exfoliation of several grains, the maximum grain area being <0.02 μm^2 as estimated from the lateral size of the grains. The total area occupied by the pits is 13.3 μm^2 which amounts to ~13% of the analyzed surface (100 μm^2). The major part of the pits measured in Fig. 12a have a depth ranging from 30 to 50 nm. This is of the order of the lateral size of the smaller grains measured on the pristine oxide surface and suggests that only the topmost layer consisting of V_2O_5 grains has been removed from the film by exfoliation.

Fig. 14 shows two AFM images obtained after 2450 cycles during the 4500 cycle test. On this sample, the oxide layer also shows grain exfoliation but the pit area distribution is different as shown in Fig. 15. There are only 4 pits with an area larger than 0.5 μm^2. The number of pits ranging from 0.2 to 0.5 μm^2 is 15 whereas the number of pits smaller than 0.2 μm^2 is about 150. The total area occupied by the pits is 9.1 μm^2, which amounts to ~9% of the analyzed surface (100 μm^2). The smaller pits obtained in this test suggest a different mechanism of grain exfoliation, most likely related to the microstructure of the pristine oxide film. It can be seen in Fig. 14b that the pits

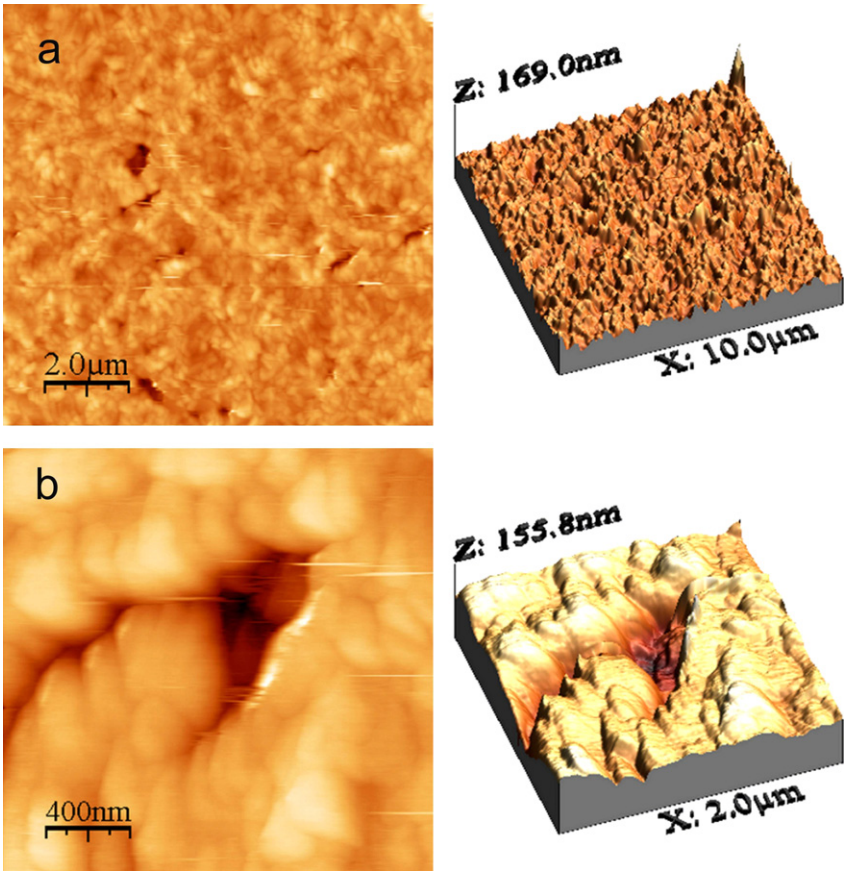

Fig. 14. Topographic AFM images of the V_2O_5/V(1 1 1) thin film after 2450 CV's: (a) 10 $\mu m \times 10$ μm and (b) 2 $\mu m \times 2$ μm. Topview (left) and 3D view (right).

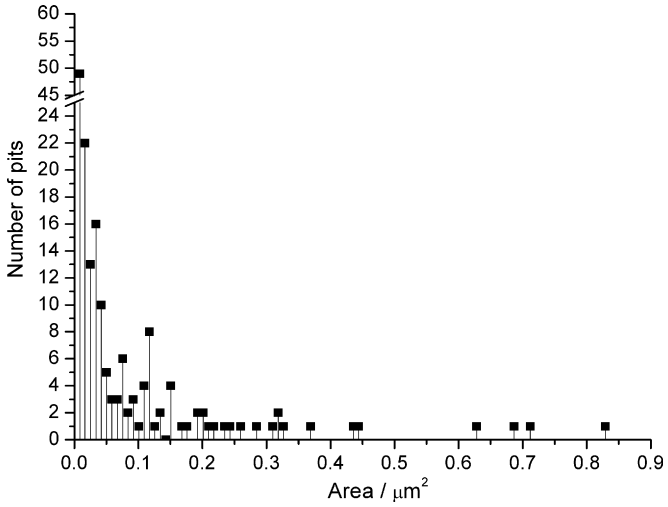

Fig. 15. Pit area histogram calculated from the AFM image in Fig. 14a by selecting a minimum depth of the pits of 50 nm and minimum area of 0.0015 μm^2.

are elongated along the grain boundaries. Fig. 14a shows more elongated pits. Their dimensions range from 100 to 150 nm in width (measured at the surface) and from 30 to 90 nm in depth. The width suggests that the exfoliation can propagate grain-by-grain along the grain boundaries. The depth suggests that the exfoliation can be limited to the V_2O_5 outer layer of the oxide film, measured by RBS to a depth of ~77 nm on this sample. Exfoliation can also reach the V_6O_{13} inner layer, measured by RBS to a depth of ~138 nm on this sample. The larger triangular pit in Fig. 14b has a total depth of 120 nm with a first level at 40 nm. This indicates that the process of exfoliation proceeds inwards in the oxide film, reaching the inner layer consisting of V^{4+} ions according to RBS. The grains appear much less sharp after 2450 cycles with grain boundaries much less well-defined than on the pristine oxide.

After 4500 cycles of Li intercalation/de-intercalation, the AFM analysis was made uncertain due to the fact that the set-up inside the glove box does not allow to select the surface region to be analyzed. Different random analyses of the sample surface were attempted. The majority of the images showed major modifications of the topography. Fig. 16 presents a typical example where the surface appears amorphous with small grains having no well-defined crystalline shapes. It possibly corresponds to residues of the oxide film remaining on the surface after stripping.

4. Discussion

In the following, we combine the electrochemical, AFM, RBS and XPS data presented above and compare them with previous results obtained after one cycle of Li intercalation/de-intercalation [28] to discuss the mechanism of capacity fading after multi-cycling.

The capacity fading in the 700 cycle test is about 16%. The XP V 2p core level spectra show a modified concentration of the outer surface of the oxide film which is 77% V^{5+} and 23% V^{4+} after 700 cycles. In order to deduce the variation due to cycling, the concentration of V^{4+} must be corrected from the initial concentration of the pristine surface (5% in this test), but also from the additional concentration of 8% of V^{4+} due to Li remaining in the oxide film after the first intercalation/de-intercalation cycle in the same safe potential range [28]. After 700 cycles, the additional fraction of V^{4+} measured at the surface of the oxide film can then be estimated to ~10%. This additional fraction can result from more Li trapped in the outer V_2O_5 layer or from the measurement of the inner layers of the oxide film containing V^{4+} ions.

The AFM analysis after 700 cycles indicates that ~13% of the surface is occupied by pits produced by grain exfoliation. The pit depth is consistent with the exfoliation of the grains forming the outer V_2O_5 layer of the oxide film but is lower than the total thickness of the film containing V^{5+} and V^{4+} ions. It suggests that the bottom of the pits corresponds to the V_6O_{13} inner layer of the oxide film. The fact that grain exfoliation has not proceeded further inwards in the oxide film is supported by the absence of V^{3+} or lower oxidation state components measured in the XP V 2p spectrum. Therefore, it can be concluded that ~13% of the surface measured by AFM corresponds to the bottom of the pits constituted of V^{4+} ions, in good agreement with the additional fraction of ~10% of the surface vanadium ions being V^{4+} as measured by XPS after 700 cycles. The capacity fading of 16% can then be related to the loss of electro-active material affecting

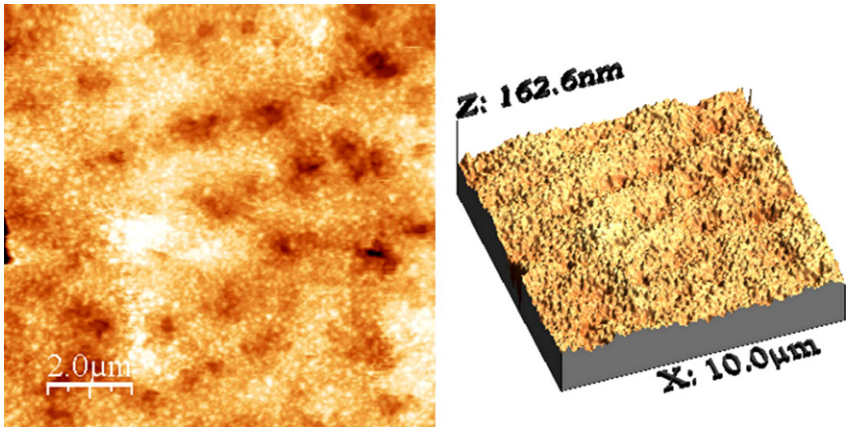

Fig. 16. Topographic AFM image of the V_2O_5/V(1 1 1) surface after 4500 cycles. Topographic and 3D views are shown. Topview (left) and 3D view (right).

∼13% of the active surface as measured by AFM. Thus, these combined measurements allow to conclude that this is the loss of electro-active material by grain exfoliation rather than the reduction of the oxide film that would be the primary cause of capacity fading.

In the 4500 cycle test, the capacity fading reaches 9% after 700 cycles and 18% after 1200 cycles. It is stable between 1200 and 2450 cycles. The XP V 2p spectra obtained after 1200 and 2450 cycles show that 27 and 16% of the surface vanadium ions are V^{4+}, respectively. This respectively amounts to 15 and 4% after correction from the fraction of V^{4+} ions initially present (4% in this case) and from the additional fraction (8%) of V^{4+} found after the first intercalation/de-intercalation cycle [28]. The decrease of these values with cycling, whereas the capacity fading increases, supports the above conclusion that capacity fading does not result from the reduction of the oxide film. The higher value of 15% of additional V^{4+} after 1200 cycles suggests that an excess of Li ions remains intercalated in the oxide film, but not irreversibly since this value decreases upon further cycling. The XP C 1s and O 1s core level spectra show the presence of lithium carbonates and Li-alkyl carbonates and/or Li-alkoxides revealing the formation of the SEI layer. These species were also observed after the first intercalation/de-intercalation cycle [28]. The photoelectron intensity originating from these species does not vary markedly when comparing the data obtained after 1, 1200 and 2450 cycles, indicating that the capacity fading after 2450 cycles does not result from the dissolution and/or conversion with cycling of the SEI layer.

The AFM images show that the process of grain exfoliation also takes place, albeit producing a pit distribution different from that obtained after 700 cycles. After 2450 cycles, only a small fraction (estimated to ∼6% from the histogram in Fig. 15) of the surface corresponds to enlarged pits having a depth consistent with the exfoliation of the V_2O_5 outer layer of the oxide film. The fraction of 4% of V^{4+} ions produced after 2450 cycles in this test could correspond to the VO_2 inner layer of the oxide film revealed at the bottom of the enlarged pits by the exfoliation of the V_2O_5 outer grains. The AFM images also show the formation of narrow and elongated pits running along the grain boundaries. Their depth are also consistent with the exfoliation of single V_2O_5 grains from the outer layer of the oxide film. The total area of the pits is ∼9% of the surface, in less good agreement with the capacity fading of ∼18% measured at this stage.

After 3300 cycles, the capacity dropped to ∼25% of the initial value. The XPS data indicate a surface very similar to that obtained after 2450 cycles except for the C 1s core level, which suggests a possible dissolution or conversion of the SEI layer since Li carbonates are no longer observed. After 4500 cycles, the heterogeneity of the surface observed at the macroscopic scale was confirmed by XPS. Although some sites of the surface have a vanadium composition close to that observed after 2450 and 3300 cycles, other sites reveal a severe loss of oxide material allowing to measure the metallic signal of the substrate. This is consistent with the exfoliation of grains observed in the previous stages and show that the process can progress inwards in the oxide film to expose the metal surface. It should be mentioned that the process of rinsing with acetonitrile may also facilitate the grains exfoliation [6].

The grain exfoliation process evidenced in this study suggests a major role of the grain boundaries. A distortion of the V_2O_5 lattice is induced by the transition from the α to the δ phase. Indeed, the planes formed by the VO_5 truncated octahedra in α-V_2O_5 become corrugated in the δ phase to accommodate the Li ions [3,4]. This distortion is reflected by the increase of the FWHM values already observed after intercalation during the first cycle [28] and confirmed in the present study after multi-cycling. From the structure of the α and δ phases [3,4], it can be deduced that the $\alpha \rightarrow \delta$ phase transition is accompanied by a volume increase of 11.5% of the oxide lattice, which is likely to cause compressive stress at the grain boundaries. Cycling the $\alpha \rightarrow \delta$ phase transition is then expected to cycle the stress generated at grain boundaries and thus to promote the de-cohesion of the grains leading to exfoliation.

The loss of grain boundary material after cycling has recently been reported for sol–gel V_2O_5 thin films [6]. The presence of poorly crystalline (amorphous) material in the as-received oxide films was advanced to explain the loss of material at grain boundaries after cycling and rinsing. The amorphisation of the oxide structure at grain boundaries after cycling cannot be excluded in our case. The more rounded morphology of the grains with grain boundaries less well-defined observed by AFM after cycling possibly correspond to the amorphisation of the structure initiated at the grain boundaries.

It cannot be excluded that the dissolution and/or conversion of the SEI layer measured after 3300 cycles contribute to the capacity drop observed at this stage. The growth of the SEI layer and its variations have been discussed recently [7]. The SEI layer acts as protective layer permeable to Li cations but not to other electrolyte components. The growth of "non-SEI" layers of different compositions is also possible [7]. The breakdown of the protective SEI layer has also been advanced as a result of structural modifications like amorphisation generated by multi-cycling [7]. In the case of amorphous V_2O_5 thin film, the dissolution of passivating layer, mainly consisting of Li_2CO_3, has been observed upon charging [20]. The breakdown of the SEI layer may also be induced by the strain generated between the oxide particles by multi-cycling.

The conversion or/and dissolution of the SEI layer can also be a result of the presence of contaminants originating from the glass/Teflon electrochemical cell. The presence of Na, K and F was observed in the survey spectra after 4500 cycles. These contaminants account for the presence of a small intensity oxygen peak at $E_B(O\ 1s_D) = 533.58$ eV. A restructuring of damaged SEI layer is also possible [7], which could be the case after 4500 cycles in Points 1 and 2 where the presence of Li_2CO_3 was observed.

5. Conclusion

SSCV, XPS and AFM were combined in two multi-cycling tests (700 and 4500 cycles) of Li intercalation/de-intercalation to study the ageing mechanisms of V_2O_5 thin films formed by thermal oxidation of vanadium metal and characterized by

RBS. XPS analysis was performed using a direct anaerobic and anhydrous transfer of the samples from the Ar atmosphere of the glove box, where the electrochemical intercalation was performed (in 1 M $LiClO_4$), to the ultra-high vacuum environment of the XPS spectrometer. AFM imaging was performed in the Ar atmosphere of the glove box.

SSCV shows quite stable Li intercalation properties of the V_2O_5 thermal oxide thin films over the first two thousands cycles in the safe potential range ($E \in [3.8, 2.8\ V]$ versus Li/Li^+), with a capacity fading lower than 20%. Combined XPS, RBS and AFM analysis show that the loss of V_2O_5 active material is the major cause of capacity fading in this stage of cycling. AFM reveals pits, the dimensions of which are consistent with the exfoliation of V_2O_5 crystalline grains forming the outer layer of the thermal oxide film. The exposed bottom of the pits corresponds then to the inner layer of the oxide film and consists of VO_2 (or mixed VO_2 and V_2O_5) as deduced from the increased V^{4+} content of the surface measured by XPS. AFM images show that grain exfoliation results from the de-cohesion of the oxide film at grain boundaries. De-cohesion can result from the strain generated by repeated lattice distortions (reflected by the changes of FWHM in XPS) and the associated expansions/contractions of volume produced when cycling through the α-to-δ phase transition. Other changes like the partial reduction of V^{5+} to V^{4+} ions, due to Li remaining intercalated in the V_2O_5 oxide film, and the formation at the surface of the so-called SEI layer containing Li carbonates and/or Li-alkoxides and Li-alkyl carbonates, also observed after the first intercalation/de-intercalation cycle, are not amplified after 2450 cycles.

After 3300 cycles, the dissolution and/or conversion of the SEI layer is characterized by the disappearance from the surface of the Li carbonate species. It can contribute to the capacity fading reaching ∼25% at this stage. The breakdown of the SEI layer could be induced by the strain generated by repeated lattice distortions and a possible amorphisation initiated at the grain boundaries as suggested by the more rounded morphology of the grains observed by AFM. After 4500 cycles, the oxide film became inhomogeneous at the macroscopic scale and very labile due to further de-cohesion. It could be stripped away by rinsing to reveal the vanadium metal substrate.

Acknowledgements

This work was supported by the European Community within the European Network "INTERCALNET" (HPNR-CT-2002-00329). The RBS experiments were possible thanks to the cooperative structure around SAFIR.

References

[1] J.S. Braithwaite, C.R.A. Catlow, J.D. Gale, J.H. Harding, Chem. Mater. 11 (1999) 1990.
[2] I. Loa, A. Grzechnik, U. Schwarz, K. Syassen, M. Han, P.K. Kremer, J. Alloys Compd. 317 (2001) 103.
[3] D.W. Murphy, P.A. Christian, F.J. Disalvo, J.V. Waszczak, Inorg. Chem. 18 (1979) 2800.
[4] J.-M. Cocciantelli, J.-P. Doumerc, M. Pouchard, M. Broussely, J. Labta, J. Power Sources 34 (1991) 103.
[5] V. Vivier, J. Farcy, J.P. Pereira-Ramos, Electrochim. Acta 44 (1998) 831.
[6] D. Alamarguy, J.E. Castle, N. Ibris, A.M. Salvi, Surf. Interf. Anal. 38 (2006) 801.
[7] J. Vetter, P. Novak, M.R. Wagner, C. Veit, K.-C. Moller, J.O. Besenhard, M. Winter, M. Wohlfart-Mehrens, C. Vogler, A. Hammouche, J. Power Sources 147 (2005) 269.
[8] A.N. Day, B.P. Sullivan, US Patent 3,655,585 (1972).
[9] H.-K. Park, W.H. Smyrl, J. Electrochem. Soc. 142 (1995) 1068.
[10] D.B. Le, S. Passerini, A.L. Tipton, B.B. Owens, W.H. Smyrl, J. Electrochem. Soc. 142 (1995) L102.
[11] J.-P. Pereira-Ramos, N. Baffier, G. Pistoia, in: G. Pistoia (Ed.), Lithium Batteries: New Materials, Developments and Perpectives, Elsevier, Amsterdam, 1994, p. 281.
[12] N. Kumagai, K. Tanno, T. Nakajima, N. Watanabe, Electrochim. Acta 28 (1983) 17.
[13] J.-G. Zhang, J.M. McGraw, J. Turner, D. Ginley, J. Electrochem. Soc. 144 (1997) 1630.
[14] A. Mantoux, H. Groult, E. Balnois, P. Doppelt, L. Gueroudji, J. Electrochem. Soc. 150 (2004) A368.
[15] F. Lantelme, A. Mantoux, H. Groult, D. Lincot, J. Electrochem. Soc. 150 (2003) A1202.
[16] F. Donsati, K. Kostourou, F. Decker, N. Ibris, A.M. Salvi, M. Liberatore, A. Thissen, W. Jeagerman, D. Lincot, Surf. Interf. Anal. 38 (2006) 815.
[17] J.A. Theil, E. Kusamo, A. Rockett, Thin Solid Films 133 (1998) 122.
[18] T. Szorenyi, K. Bali, I. Hevesi, J. Non-Cryst. Solids 35-36 (1980) 1245.
[19] K. Inumaru, T. Okuhara, M. Misono, N. Matsubayashi, H. Shimada, A. Nishijima, J. Chem. Soc. Faraday Trans. 88 (1992) 625.
[20] A. Benayad, H. Martinem, A. Gies, B. Pecquenard, A. Levasseur, D. Gonbeau, J. Electron Spectrosc. Relat. Phenom. 150 (2006) 1.
[21] S. Lu, L. Hou, F. Gan, J. Mater. Sci. 28 (1993) 2169.
[22] J.-S. Bae, S.-I. Pyun, J. Alloys Compd. 217 (1995) 52.
[23] S. Deki, Y. Aoi, Y. Miyake, A. Gotoh, A. Kajinami, Mater. Res. Bull. 31 (1996) 1399.
[24] E. Poitron, A. LeGal LaSalle, S. Sarciaux, Y. Piffard, D. Guyomard, J. Power Sources 81 (1999) 666.
[25] E. Andrukaitis, J. Power Sources 119–121 (2003) 205.
[26] R. Lindstrom, V. Maurice, S. Zanna, L. Klein, H. Groult, L. Perrigaud, C. Cohen, P. Marcus, Surf. Interf. Anal. 38 (2006) 6.
[27] R. Lindstrom, V. Maurice, H. Groult, L. Perrigaud, S. Zanna, C. Cohen, P. Marcus, Electrochim. Acta 51 (2006) 5001.
[28] J. Światowska-Mrowiecka, V. Maurice, S. Zanna, L. Klein, P. Marcus, Electrochim. Acta 52 (2007) 5644.
[29] M.D. Levi, Z. Lu, D. Aurbach, Solid State Ionics 143 (2001) 309.
[30] G. Beamson, D. Briggs, High Resolution XPS of Organic Polymers, The Scienta ESCA 300 Database, John Wiley & Sons, 1992.
[31] S.L.T. Anderson, J. Chem. Soc. Faraday Trans. 175 (1979) 1356.
[32] J. Mendialdua, R. Casanova, Y. Barbaux, J. Electron Spectroc. Relat. Phenom. 71 (1995) 249.
[33] D. Aurbach, B. Markovsky, A. Shechter, Y. Ein-Eli, H. Cohen, J. Electrochem. Soc. 143 (1996) 3809.
[34] G.R. Zhuang, K. Wang, Y. Chen, P.N. Ross Jr., J. Vac. Sci. Technol. A 16 (1998) 3041.
[35] M. Herstedt, A.M. Andersson, H. Rensmo, H. Siegbahn, K. Edstrom, Electrochim. Acta 49 (2004) 4939.
[36] E. Peled, J. Electrochem. Soc. 126 (1979) 2047.
[37] E.C. Almeida, M. Abbate, J.M. Roselen, Solid State Ionics 140 (2001) 241.